Revista de Metalurgia
October–December 2018, 54 (4), e129
ISSN-L: 0034-8570
https://doi.org/10.3989/revmetalm.129

Structural studies of evolution of solid solutions of $BaTiO_3$ doped with Er^{3+} (solid-state reaction method)

Miguel Pérez-Labra[a,✉], Francisco R. Barrientos-Hernández[a], Juan P. Hernández-Lara[a], José A. Romero-Serrano[b], Martín Reyes-Pérez[a], Víctor E. Reyes-Cruz[a], Julio C. Juárez-Tapia[a], Gustavo Urbano-Reyes[a]

[a]Academic Area of Earth Sciences and Materials, Autonomous University of Hidalgo State. Road Pachuca- Tulancingo Km 4.5 Mineral de la Reforma, Zip Code 42184, Hidalgo México
[b]Metallurgy and Materials Department, ESIQIE-IPN. UPALM, Zacatenco, Zip Code 07738, Ciudad de México, México

(✉Corresponding author: miguelabra@hotmail.com)

Submitted: 28 November 2017; Accepted: 20 February 2018; Available On-line: 2 October 2018

ABSTRACT: Erbium doped $BaTiO_3$ compositions were synthetized using the conventional solid-state method in air atmosphere, according to the general formula $Ba_{1-x}Er_xTi_{1-x/4}O_3$ and x = 0.0, 0.003, 0.005, 0.01, 0.05, 0.1, 0.15, 0.20, 0.25, 0.30, 0.35 Er^{3+} (wt. %). $BaTiO_3$:Er^{3+} were prepared using barium carbonate [$BaCO_3$], titanium oxide [TiO_2] and erbium oxide [Er_2O_3] as precursors. The powders were decarbonated at 900 °C for 12 h and sintered at 1400 °C for 12 h. The structural evolution of solid solutions was monitored by X-ray diffraction, Raman spectroscopy, Infrared spectroscopy and scanning electron microscopy. The results showed that the crystal phase of the particles obtained was predominately tetragonal $BaTiO_3$. A secondary phase identified as a pyrochlore ($Er_2Ti_2O_7$) was found when the Er^{3+} content was higher than 0.05 wt. %. The solubility limit of Er^{3+} in the crystal structure of $BaTiO_3$ was reached when x was = 0.05. The results obtained by MEB-EDS indicated the incorporation of erbium in the crystalline structure of $BaTiO_3$. The IR results showed no absorption bands contamination of O-H group into the products.

KEYWORDS: $BaTiO_3$; Doping; Er^{3+}; Sintering

Citation/Citar como: Pérez-Labra, M.; Barrientos-Hernández, F .R.; Hernández-Lara, J .P.; Romero-Serrano, J.A.; Reyes-Pérez, M.; Reyes-Cruz, V.E.; Juárez-Tapia, J.C.; Urbano-Reyes, G. (2018). "Structural studies of evolution of solid solutions of $BaTiO_3$ doped with Er^{3+} (solid-state reaction method)". *Rev. Metal.* 54(4): e129. https://doi.org/10.3989/revmetalm.129

RESUMEN: *Estudios de evolución estructural de soluciones solidas de $BaTiO_3$ dopadas con Er^{3+} (método de reacción en estado sólido)*. Se sintetizaron composiciones de $BaTiO_3$ dopadas con erbio empleando el método convencional de reacción en estado sólido en atmosfera de aire, de acuerdo a la formula general $Ba_{1-x}Er_xTi_{1-x/4}O_3$ y x = 0,0; 0,003; 0,005; 0,01; 0,05; 0,1; 0,15; 0,20; 0,25; 0,30; 0,35 Er^{3+} (% peso). Las muestras de $BaTiO_3$ dopadas con Er^{3+} fueron preparadas usando carbonato de bario [$BaCO_3$], óxido de titanio [TiO_2] y óxido de erbio [Er_2O_3] como precursores. Los polvos fueron decarbonatados a 900 °C por 12 h y sinterizados a 1400 °C por 12 h. La evolución estructural de las soluciones sólidas fue monitoreada por difracción de rayos X (DRX), espectroscopia Raman (ER), espectroscopia de infrarrojo (EI) y microscopía electrónica de barrido (MEB-EDS). Los resultados mostraron que la fase cristalina de las partículas obtenidas fue $BaTiO_3$ predominantemente tetragonal. Se encontró una fase secundaria identificada como pirocloro ($Er_2Ti_2O_7$) cuando el contenido de Er^{3+} en las muestras fue mayor que 0,05 % peso. El límite de solubilidad de Er^{3+} en la estructura cristalina del $BaTiO_3$ se alcanzó cuando x fue = 0,05. Los resultados obtenidos por MEB-EDS indicaron la incorporación de erbio en la estructura cristalina del $BaTiO_3$. Los resultados de EI no mostraron bandas de contaminación de grupos O-H en los productos obtenidos.

PALABRAS CLAVE: $BaTiO_3$; Dopaje; Er^{3+}; Sinterización

ORCID ID: Miguel Pérez-Labra (https://orcid.org/0000-0001-9882-6932); Francisco R. Barrientos-Hernández (https://orcid.org/0000-0001-5459-7162); Juan P. Hernández-Lara (https://orcid.org/0000-0003-2937-7349); José A. Romero-Serrano (https://orcid.org/0000-0001-9324-5602); Martín Reyes-Perez (https://orcid.org/0000-0003-3843-2397); Víctor E. Reyes-Cruz (https://orcid.org/0000-0003-2984-850X); Julio C. Juárez-Tapia (https://orcid.org/0000-0001-7058-1670); Gustavo Urbano-Reyes (https://orcid.org/0000-0001-5461-4030)

1. INTRODUCTION

Barium titanate ($BaTiO_3$) is a ferro-electric material that can be formulated in a large number of systems and solid solutions that provide a wide range of various applications. The ferro-electric (tetragonal) phase gets converted into para-electric (cubic) phase at the Curie temperature (Tc) at ~ 120 °C for single-crystals. Its structure type perovskite has the capability to host ions of different sizes; so, an important number of distinct dopants can be accommodated in the $BaTiO_3$ lattice, which makes $BaTiO_3$ semi-conducting (Vijatović *et al.*, 2010). The doping process of $BaTiO_3$-based ceramics is of great value in the production of electric and electronic devices (multilayer capacitors, piezoelectric transducers sensors with positive temperature coefficient of resistivity etc.) (Jaffe, 1971; Moulson and Herbert, 2003). The $BaTiO_3$ doping process with rare earth ions has been of interest to many researchers, who have found significant improvements in its electrical properties (Pinceloup *et al.*, 1999; Durán *et al.*, 2001; Hwang *et al.*, 2004; Zhao *et al.*, 2006; Hao *et al.*, 2011; Zhang *et al.*, 2011; Yan-Xia *et al.*, 2012; Zhang and Hao, 2013). Specifically, erbium, (trivalent lanthanide element) has been mainly researched as a dopant in optical fiber amplifiers (Tsur *et al.*, 2001; Yongping *et al.*, 2007; Markom *et al.*, 2017), where it showed excellent properties. As a dopant in $BaTiO_3$, nanoparticles have been synthesized using the hydrothermal method, generating a stable cubic phase below 30 nm in size (Garrido-Hernández *et al.*, 2014). The structure of $BaTiO_3$ is of great importance, because its properties depend on its crystallographic phase. The cubic phase has para-electric properties, and the tetragonal phase does not exhibit these properties (Kao, 2004; Carter and Norton, 2007).

In doping, the multiple occupation of ions in the sites A or B in the ABO_3 compounds affect the Curie's temperature and other physical properties (Zhang *et al.*, 2011). The incorporation of isovalent impurities it has no effect on the population of defects; however, the anisovalent impurities (valence different from that of those it replaces) require the formation of opposite charge compensation defects to maintain electrical neutrality. If the replacement cation has a lower valence than the original, electronic holes could free themselves and if the replacement cation has a valence greater than the original cation could release electrons (an *electron hole* or is the lack of an electron at a position where one could exist in an atom or atomic lattice) (Chan *et al.*, 1986). It is noted that both the valence state and the radius of Er^{3+} ion (1.00 Å) are intermediate between those of Ba^{2+} ion (1.42 Å) and Ti^{4+} ion (0.61 Å). As a result, theoretically Er^{3+} can occupy either A or B site, depending on Ba/Ti mole ratio (Takada *et al.*, 1987; Dunbar *et al.*, 2004; Mitic *et al.*, 2010; Zhang and Hao, 2013). Then, if Er^{3+} is added at the $BaTiO_3$ it would have (Chan *et al.*, 1986) Eq. (1):

$$Er_2O_3\,(\text{en } BaTiO_3) \rightarrow 2Er^{\bullet}_{Ti} + 2O_o + (1/2)\,O_2\,(g) + 2e' \quad (1)$$

Based on the above, the structural behavior of $BaTiO_3$ may be affected; this is why this study addresses the effect of the addition of Er^{3+} on the structural characteristics of $BaTiO_3$. The amount of added erbium will be varied between 0.003 and 0.35 (wt. %) to know the limit of solubility of erbium in $BaTiO_3$. The method used is the solid state reaction, which is an important technique in the preparation of polycrystalline solids. A solid state reaction, also called dry reaction mixture of oxides, is a chemical reaction in which no solvents are used. The advantages of this method (compared to other techniques) are mainly economic and, hence large scale production is frequently based on solid-state reactions of mixed powders (Hernández Lara *et al.*, 2017).

2. EXPERIMENTAL PROCEDURE

Samples of $BaTiO_3$ doped with Er^{3+} were elaborated using the solid-state reaction method, by grinding stoichiometric amounts of $BaCO_3$ (Sigma-Aldrich CAS No. 513-77-9 99.0%), TiO_2 (Sigma Aldrich CAS No. 1317-80-2 99.99%) and Er_2O_3 (Sigma-Aldrich CAS Number: 12061-16-4 99.99%) in an agate mortar, with acetone as a control medium according to the equation $Ba_{1-x}Er_xTi_{1-x/4}O_3$ and x = 0, 0.003, 0.005, 0.01, 0.05, 0.1, 0.15, 0.20, 0.25, 0.30, 0.35 Er^{3+} (wt. %). The powders ($BaCO_3$, TiO_2 and Er_2O_3) were previously dried in a muffle-type oven for 24 h at 200 °C before weighting. The mixture was decarbonated at 900 °C for 12 h using an Al_2O_3 crucible as a container, and subsequently ground again for 30 min in an agate mortar. The powder mixture obtained was sintered at 1400 °C for 12 h in a platinum crucible in air atmosphere with heating and cooling rates of 5 °C·min^{-1}, using a muffle furnace (Thermolyne model 46200). The powder mixes were ground again for 30 min in an agate mortar and then compacted using uniaxial pressing at 250 MPa in an 8-mm stainless steel die, to produce green pellets of approximately 3 mm thickness. The pellets were sintered at 1400°C for 5 h in air atmosphere with heating and cooling rates of 5 °C·min^{-1}. The structural evolution of the products was evaluated and monitored using X-ray diffraction (diffractometer Equinox 2000 Cu Kα). The analysis of the morphology in the pellets sintered was carried out using a

JEOL 6300 SEM. Raman studies for each sample obtained after sintering were performed in a spectrophotometer (Perkin Elmer Spectrum Gx) over the range of 100–1200 wavelength (cm^{-1}). Additionally, to determine contamination of O-H group into the products, IR spectra were recorded for the samples with more significant results in the previous techniques using a Perkin Elmer 2000 FT-IR in the range 700–400 cm^{-1}.

3. RESULTS AND DISCUSSION

3.1. X-Ray diffraction

The X-ray diffraction patterns of $BaTiO_3$ doped with Er^{3+} are shown in Fig. 1. A combination of cubic (JCPDS 310174) and tetragonal phases (JCPDS 050626), with the latter being predominant, was obtained. It can be seen from the X-Ray patterns that when Er^{3+} content was $0.003 \leq x \leq 0.35$, the presence of a double peak located at $2\theta \approx 46°$, indicates the existence of the tetragonal phase (JCPDS 050626) (Hernández Lara *et al.*, 2017), which, as mentioned above, exhibits ferroelectric properties. On the other hand, it can also be noted that when the concentration of Er^{3+} was $x > 0.05$, a secondary phase identified as $Er_2Ti_2O_7$ (JCPDS 731647) was detected in the peaks located at $2\theta \approx 28°$, $2\theta \approx 29.6°$ and $2\theta \approx 35.36°$ (Fig. 2). It has been reported (Li *et al.*, 2012), that pyrochlores $A_2B_2O_7$ belong to Fd3m space group, and are a superstructure of the fluorite structure (MO_2) but with two cations and one eighth of the oxygen anion absent. Pyrochlores $A_2B_2O_7$ are important candidates as ceramic waste forms for actinide immobilization and are among the principal host phases currently considered for the disposition of Pu from dismantled nuclear weapons and the "minor" actinides (Yashima *et al.*, 1996; Dobal and Katiyar, 2002). The formation of the secondary phase ($Er_2Ti_2O_7$) indicates that the solubility limit of Er^{3+} in the $BaTiO_3$ crystal structure is reached when $x = 0.05$. Additionally, Fig. 3 shows the sizes of crystallites obtained for each composition estimated from the broadening of the diffraction deflections, by applying the Scherrer equation, (Eq. (2)):

$$t = \frac{k\lambda}{B\cos\theta} \tag{2}$$

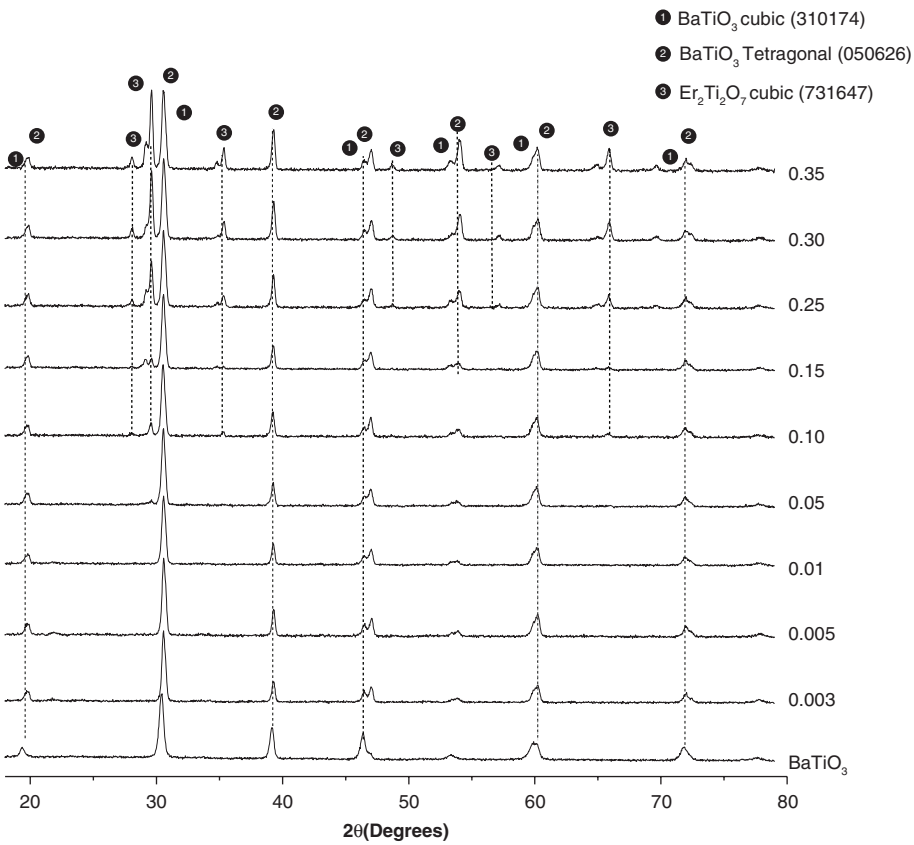

FIGURE 1. XRD diffractograms for $Ba_{1-x}Er_xTi_{1-x/4}O_3$ powders sintered at 1400 °C for 5 h for different values of x.

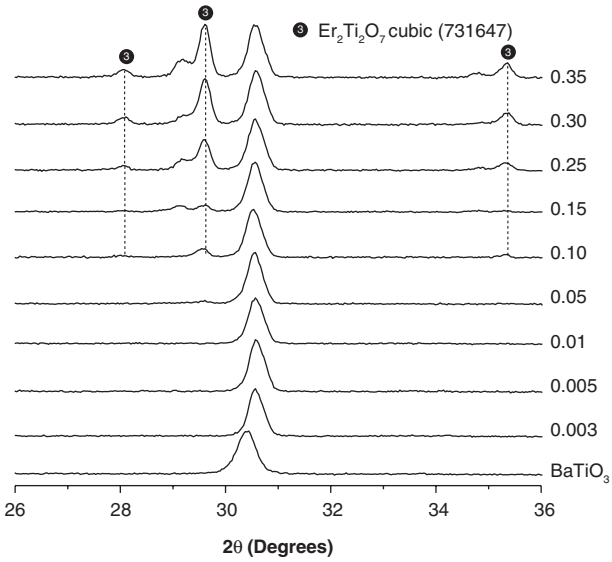

FIGURE 2. XRD diffractograms for $Ba_{1-x}Er_xTi_{1-x/4}O_3$ powders sintered at 1400 °C for 5 h for different values of x, zoom at 26-36°.

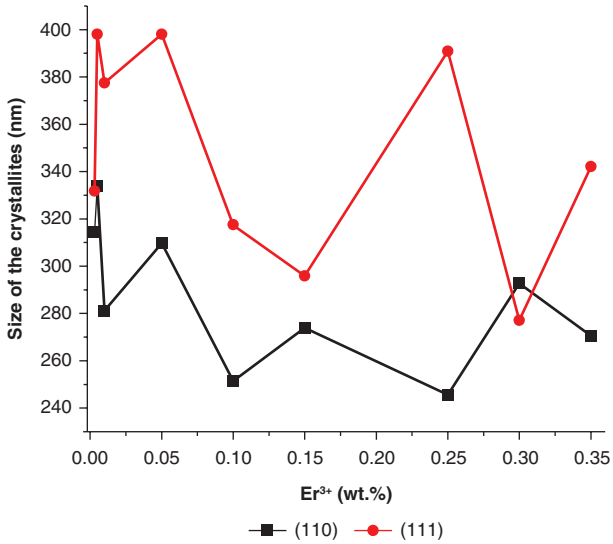

FIGURE 3. Sizes of crystallites obtained for powders sintered at 1400 °C for 5 h for different values of x.

Where: t = grain size, λ = wavelength, B = is the line broadening at half the maximum intensity (FWHM), after subtracting the instrumental line broadening, in radians. This quantity is also sometimes denoted as $\Delta(2\theta)$, θ= Bragg angle (in degrees), k = form factor (constant = 1.15).

The estimated average sizes were ~285.9 nm for (110), and 347.6 nm for (111) planes respectively. The absence of trend observed in Fig. 3 can be attributed to the radius of Er^{3+} ion being intermediate between those of Ba^{2+} ion and Ti^{4+} ion. Thereby, the Er^{3+} could have occupied the A or B site (Zhang *et al.*, 2011).

3.2. Raman spectroscopy

Raman spectroscopy is a spectroscopic technique used to observe vibrational, rotational, and other low-frequency modes in a system. This has the ability to be very sensitive to transitions involving oxygen displacements and can detect the local lattice distortions and crystallographic defects at the molecular level (Yashima *et al.*, 1996; Dobal and Katiyar, 2002). Hence, this technique is appropriate to reveal change from the tetragonal ferroelectric phase to a cubic para-electric phase. Fig. 4 shows the evolution of Raman spectra obtained for powders of $BaTiO_3$ added to different concentrations of Er^{3+}, for $0.003 \leq x \leq 0.35$ prepared by the solid state reaction. It shows the characteristic depolarized scattering profiles for single and polycrystalline $BaTiO_3$ (Venkateswaran *et al.*, 1998).

The plots present the typical $BaTiO_3$ tetragonal phase Raman scattering bands at room temperature at about 250 (A_1(TO)), 515 (E(TO) , A_1(TO)) and 716 cm^{-1} (E(LO) , A_1(LO)) and a sharp peak at around 305 cm^{-1}(B_1, E(TO + LO)) (Asiaie *et al.*, 1996). An extra band was observed about 834 cm^{-1}, and it was noted that this occurs when Er^{3+} content was Er $0.10 \leq x \leq 0.35$. This result can be associated to the formation of the secondary phase ($Er_2Ti_2O_7$) identified in the Fig. 1 in the peaks located at $2\theta \approx 28°$, $2\theta \approx 29.6°$ and $2\theta \approx 35.36°$.

On the other hand, according to the nuclear site group analysis, (Rousseau *et al.*, 1981) Raman active phonons of the tetragonal *P4mm* (C_{4v}^1) crystal symmetry are represented by $3A_1 + B_1 + 4E$. Long-range electrostatic forces induce the splitting of transverse and longitudinal phonons, which results in split Raman active phonons represented by $3[A_1(TO)+A_1(LO)]+B_1+ 4[E(TO)+ E(LO)]$. It has been reported (Venkateswaran *et al.*, 1998) that while the cubic phase theoretically does not reveal any Raman active modes, this polymorph generally shows broad bands at around 250 and 520 cm^{-1}, which may be caused by local disorder associated with the position of Ti atoms.

3.3. Infrared spectroscopy

Infrared spectroscopy is the analysis of infrared light interacting with a molecule. It is used to determine functional groups in molecules. IR spectroscopy measures the vibrations of atoms, and based on this, it is possible to determine the functional groups.

Figure 5 shows the IR spectra for $Ba_{1-x}Er_xTi_{1-x/4}O_3$ powders sintered at 1400 °C for 5 h for x = 0 ($BaTiO_3$), 0.10 and 0.35. From the results, the characteristic absorption bands relating to $BaTiO_3$, which are

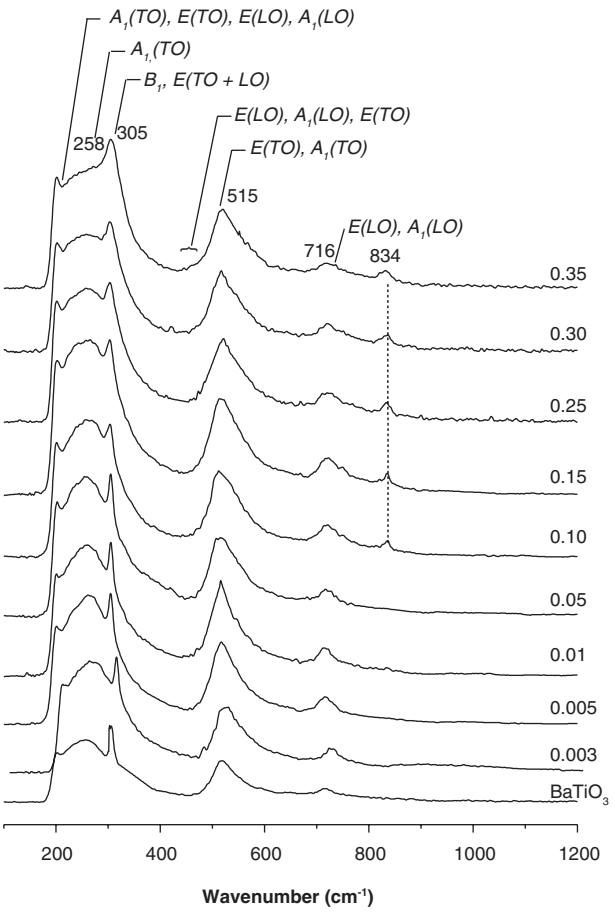

FIGURE 4. Raman spectra of sintering powders at 1400 °C, $0.003 \leq x \leq 0.35$.

located at ~545 and ~410 cm^{-1} (Asiaie *et al.*, 1996), can be clearly seen.

No bending vibrations of O-H corresponding to coordinated H_2O were observed, which validates the assumption that the synthesis method used generate pure phases of $BaTiO_3$. Garrido-Hernández *et al.* (2014) reported the presence of OH^- groups caused by the hydrolysis method used, as well as the presence of CO_3^{2-} group.

The $BaTiO_3$ is formed of Ti–O_6 octahedrons, and the Ba^{2+} is located at the center of eight Ti–O_6 octahedrons. On the other hand, the Ti–O_6 octahedron is the most stable form of Ti^{4+} and is the basic structural element in perovskite $BaTiO_3$.

3.4. Morphology and microstructure

The selected images obtained from SEM-EDS of Er^{3+} doped $BaTiO_3$ are shown in Fig. 6 for the samples sintered at 1400 °C for 5 h in air atmosphere, with heating and cooling rates of 5 °C·min^{-1} and x = 0 (a) and x = 0.25 (b). The micrographs consist of rounded grains with a wide grain-size distribution.

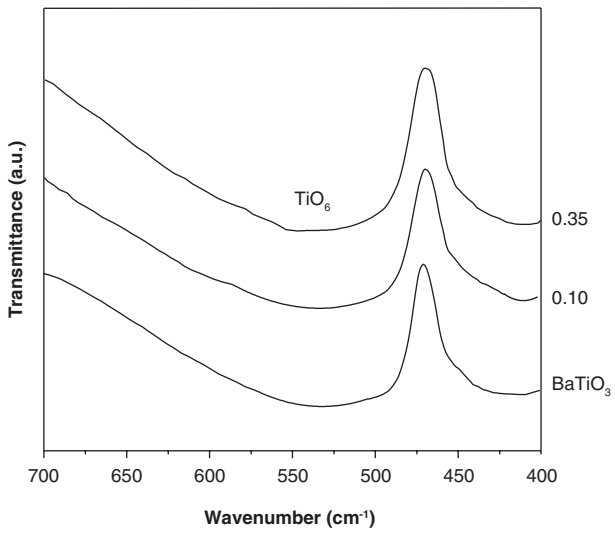

FIGURE 5. IR spectra for $Ba_{1-x}Er_xTi_{1-x/4}O_3$ powders sintered at 1400 °C for 5 h for x = 0 ($BaTiO_3$), 0.10 and 0.35.

For the undoped sample (Fig. 5 a), grain sizes average 11 μm and 6 μm for the sample with 0.25 Er^{3+} (wt. %). This figures shows that grain size diminishes when the concentration of erbium is increased. The SEM images of the sintered pellets shows that Er^{3+} did not drastically modify the microstructure. Hernández Lara *et al.* (2017) reported similar sintering structures for Gd^{3+} doped $BaTiO_3$; this can be attributed to the fact that both of them belonging to the lanthanide group. The incorporation of erbium in the crystalline structure of $BaTiO_3$ was corroborated in the EDS spectra obtained for each of the samples.

The detailed image acquired for the sample of Er^{3+} doped $BaTiO_3$ with x = 0.005 (Fig. 7) showed higher amounts of inter-granular porosity. In the same way, necks generated in the sintering process of the particles were observed.

4. CONCLUSIONS

- Structural evolution of solid solutions of Er^{3+} doping $BaTiO_3$ ($Ba_{1-x}Er_xTi_{1-x/4}O_3$) with x = 0, 0.003, 0.005, 0.01, 0.05, 0.1, 0.15, 0.20, 0.25, 0.30, 0.35 Er^{3+} (wt. %) was investigated by X-ray diffraction, Raman spectroscopy, Infrared spectroscopy, and scanning electron microscopy. A double deflexion located at $2\theta \approx 46°$ showed the formation of the tetragonal ferro-electric phase for the patterns in which Er^{3+} content was $0.003 \leq x \leq 0.35$.
- A secondary phase belonging to Fd3m space group identified as a pyrochlore ($Er_2Ti_2O_7$) was revealed at the position $2\theta \approx 28°$, $2\theta \approx 29.6°$ and $2\theta \approx 35.36°$.
- The solubility limit of Er^{3+} in the crystal structure of $BaTiO_3$ was reached when x = 0.05.

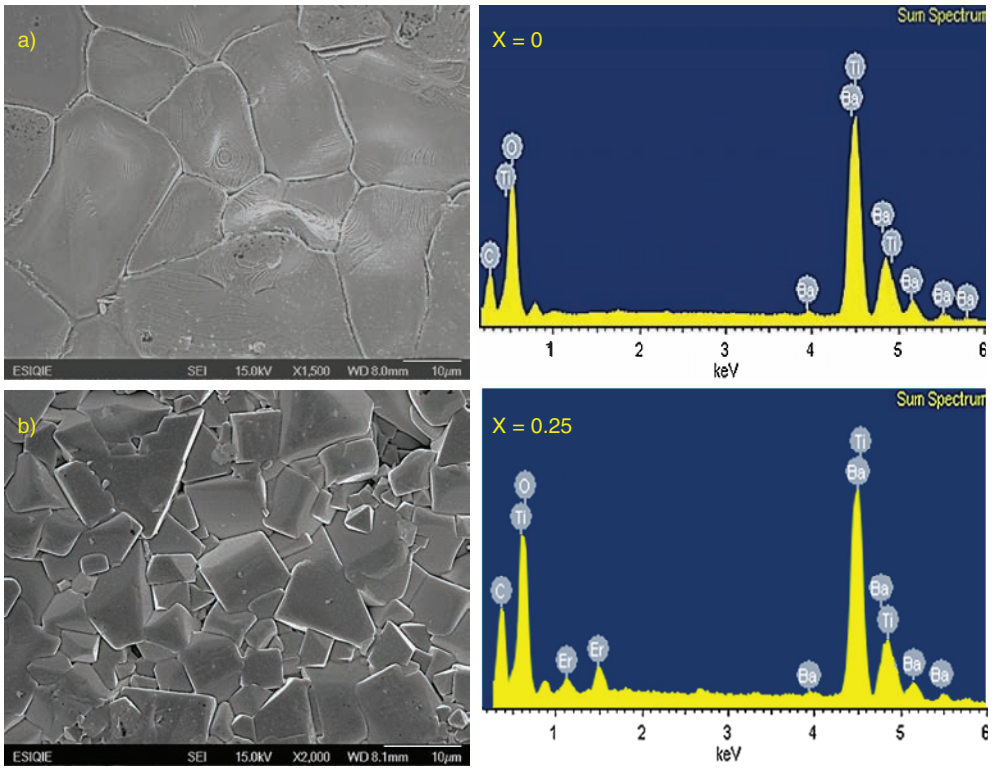

FIGURE 6. SEM-EDS micrographs of $BaTiO_3$, doped with Er^{3+}: a) x = 0.0, and b) x= 0.25.

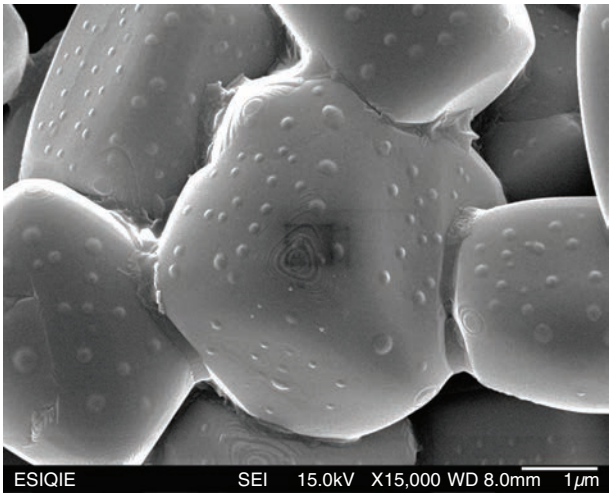

FIGURE 7. SEM micrograph detail of Er^{3+} doped $BaTiO_3$, x = 0.005.

– The Raman graphics showed the typical $BaTiO_3$ tetragonal phase scattering bands at around 250 (A_1(TO)), 520 (E(TO), A_1(TO)) and 720 cm^{-1} (E(LO), A_1(LO)) and a sharp peak at around 306 cm^{-1}(B_1, E(TO + LO)). An extra band was observed about 834 cm^{-1}, when Er^{3+} content was Er $0.10 \leq x \leq 0.35$. This result can be associated to the formation of the secondary phase ($Er_2Ti_2O_7$) identified by X-ray diffraction.
– The Infrared spectroscopy patterns indicated the characteristic absorption bands relating to $BaTiO_3$ and no absorption bands contamination of O-H group into the products was observed. The SEM micrographs consisted of rounded grains with a wide grain-size distribution. The EDS analysis confirmed the presence of the Er^{3+} in the crystalline structure of $BaTiO_3$.

ACKNOWLEDGMENT

The author is grateful to PRODEP and CONACyT-México for the financial support.

REFERENCES

Asiaie, R., Zhu, W., Akbar, S.A., Dutta, P.K. (1996). Characterization of submicron particles of $BaTiO_3$. *Chem. Mater.* 8 (1), 226–234. https://doi.org/10.1021/cm950327c.

Carter, C.B., Norton, M.G. (2007). *Ceramics Materials, Science and Engineering*. 1st. Ed. Springer, USA, pp. 562-565.

Chan, H.M., Harmer, M.R., Smyth, D.M.L. (1986). Compensating Defects in Highly Donor-Doped $BaTiO_3$. *J. Am. Ceram. Soc.* 69 (6), 507-510. https://doi.org/10.1111/j.1151-2916.1986.tb07453.x.

Dobal, P.S., Katiyar, R.S. (2002). Studies on ferroelectric perovskites and Bi-layered compounds using micro-Raman spectroscopy. *J. Raman Spectrosc.* 33 (6), 405-423. https://doi.org/10.1002/jrs.876.

Dunbar, T.D., Warren, W.L., Tuttle, B.A., Randall, C.A., Tsur, Y. (2004). Electro paramagnetic resonance investigations of lanthanide-doped barium titanate: dopant site occupancy. *J. Phys. Chem. B* 108 (3), 908-917. https://doi.org/10.1021/jp036542v.

Durán, P., Capel, F., Gutierrez, D., Tartaj, J., Bañares, M.A., Moure, C. (2001). Metal citrate polymerized complex thermal decomposition leading to the synthesis of $BaTiO_3$: effects of the precursor structure on the $BaTiO_3$ formation mechanism. *J. Mater. Chem.* 11, 1828-1836. https://doi.org/10.1039/b010172i.

Garrido-Hernández, A., García-Murillo, A., Carrillo-Romo, F. de J., Cruz-Santiago, L.A., Chadeyron, G., Morales-Ramírez, A. de J., Velumani, S. (2014). Structural studies of $BaTiO_3$:$Er^{3+}$and $BaTiO_3$:Yb^{3+}powders synthesized by hydrothermal method. *J. Rare Earth* 32 (11), 1016-1021. https://doi.org/10.1016/S1002-0721(14)60176-9.

Hao, J., Zhang, Y., Wei, X. (2011). Electric-induced and modulation of upconversion photoluminescence in epitaxial BaTiO3:Yb/Er thin films. *Angew. Chem. Int. Edit.* 50 (30), 6876-6880. https://doi.org/10.1002/anie.201101374.

Hernández Lara, J.P., Pérez Labra, M., Barrientos Hernández, F.R., Romero Serrano, J.A., Ávila Dávila, E.O., Thangarasu, P., Hernández Ramirez, A. (2017). Structural Evolution and Electrical Properties of $BaTiO_3$ Doped with Gd^{3+}. *Mater. Res.* 20 (2), 538-542. https://doi.org/10.1590/1980-5373-MR-2016-0606.

Hwang, U.Y., Park, H.S., Koo, K.K. (2004). Low-temperature synthesis of fully crystallized spherical $BaTiO_3$; particles by the gel-sol method. *J. Am. Ceram. Soc.* 87 (12), 2168-2174. https://doi.org/10.1111/j.1151-2916.2004.tb07486.x.

Jaffe, B. (1971). *Piezoelectric Ceramics*. 1st Edition, Academic Press, London, pp. 53-70.

Kao, K.C. (2004). *Dielectric Phenomena in Solids*. 1st Edition, Elsevier Academic Press, USA, pp. 221-224.

Li, Y.H., Wang, Y.Q., Xu, C.P., Valdez, J.A., Tang, M., Sickafus, K.E. (2012). Microstructural evolution of the pyrochlore compound $Er_2Ti_2O_7$ induced by lightion irradiations. *Nucl. Instrum. Meth. Phys. Res. B* 286, 218–222. https://doi.org/10.1016/j.nimb.2011.12.034.

Markom, A.M., Paul, M.C., Dhar, A., Das, S., Pal, M., Bhadra, S.K., Dimyati, K., Yasin, M., Harun, S.W. (2017). Performance comparison of enhanced Erbium–Zirconia–Yttria–Aluminum co-doped conventional erbium-doped fiber amplifiers. *Optik* 132, 75–79. https://doi.org/10.1016/j.ijleo.2016.12.041.

Mitic, V.V., Nikolic, Z.S., Pavlovic, V.B., Paunovic, V., Miljovic, M., Jordovic, B., Zivkovic, L. (2010). Influence of rare-earth dopants on barium titanate ceramics microstructure and corresponding electrical properties. *J. Am. Ceram. Soc.* 93 (1), 132-137. https://doi.org/10.1111/j.1551-2916.2009.03309.x.

Moulson, A.J., Herbert, J.M. (2003). *Electroceramics*. 2nd Edition, John Wiley and Sons, England, pp. 311-315.

Pinceloup, P., Courtois, C., Vicens, J., Leriche, A., Thierry, B. (1999). Evidence of a dissolution-precipitation mechanism in hydrothermal synthesis of barium titanate powders. *J. Eur. Ceram. Soc.* 19 (6-7), 973-977. https://doi.org/10.1016/S0955-2219(98)00356-2.

Rousseau, D.L., Bauman, R.P., Porto. S.P.S. (1981). Normal mode determination in crystals. *J. Raman Spectrosc.* 10 (1), 253-290. https://doi.org/10.1002/jrs.1250100152.

Takada, K., Chang, E., Smyth, D.M. (1987). Rare-earth addition to $BaTiO_3$. *Adv. Ceram.* 19, 147-152.

Tsur, Y., Dunbar, T.D., Randall, C.A. (2001). Crystal and defect chemistry of rare earth cations in $BaTiO_3$. *J. Electroceram.* 7 (1), 25-34. https://doi.org//10.1023/A:1012218826733.

Venkateswaran, U.D., Naik, V.M., Naik, R. (1998). High-pressure Raman studies of polycrystalline $BaTiO_3$. *Phys. Rev. B* 58 (21), 14256-14260. https://doi.org/10.1103/PhysRevB.58.14256.

Vijatović, M.M., Stojanović, B.D., Bobić, J.D., Ramoska, T., Bowen, P. (2010). Properties of lanthanum doped $BaTiO_3$ produced from nanopowders. *Ceram. Int.* 36 (6), 1817-1824. https://doi.org/10.1016/j.ceramint.2010.03.010.

Yan-Xia, L., Yao, X., Wang, X.-Sh., Hao, Y.-B. (2012). Studies of dielectric properties of rare earth (Dy, Tb, Eu) doped barium titanate sintered in pure nitrogen. *Ceram. Int.* 38 (Supp. 1), S29-S32. https://doi.org/10.1016/j.ceramint.2011.04.042.

Yashima, M., Ohtake, K., Kakihana, M., Arashi, H., Yoshimura, M. (1996). Determination of Tetragonal–Cubic Phase Boundary of $Zr_{1-X}R_XO_{2-X/2}$ (R = Nd, Sm, Y, Er and Yb) by Raman Scattering. *J. Phys. Chem. Solids* 57 (1), 17-24. https://doi.org/10.1016/0022-3697(95)00085-2.

Yongping, P., Wenhu, Y., Shoutian, Ch. (2007). Influence of rare earths on electric properties and microstructure of barium titanate ceramics. *J. Rare Earth* 25 (Supp, 1), 154-157. https://doi.org/10.1016/S1002-0721(07)60546-8.

Zhang, Y., Hao, J., Mak, C.L., Wei, X. (2011). Effects of site substitutions and concentration on upconversion luminescence of Er^{3+}-doped perovskite titanate. *Opt. Express* 19 (3), 1824-1829. https://doi.org/10.1364/OE.19.001824.

Zhang, Y., Hao, J. (2013). Color-tunable upconversion luminescence of Yb^{3+}, Er^{3+}, and Tm^{3+} tri-doped ferroelectric $BaTiO_3$ materials. *J. Appl. Phys.* 113 (8), 184112.1-184112.4. https://doi.org/10.1063/1.4805050.

Zhao, X., Ma, Z., Xiao, Z., Chen, G. (2006). Preparation and characterization on nano-sized barium titanate poder doped with lanthanum by sol-gel process. *J. Rare Earth* 24 (1), 82-85. https://doi.org/10.1016/S1002-0721(07)60329-9.